SCIENTIFIC REPORTS

OPEN

Giant proximity effect in single-crystalline MgB_2 bilayers

Soon-Gil Jung[1,2], Duong Pham[2], Tae-Ho Park[2], Han-Yong Choi[2], Jin Won Seo[3], Won Nam Kang[2] & Tuson Park[1,2]

Received: 14 November 2018
Accepted: 11 February 2019
Published online: 01 March 2019

Although giant proximity effect (GPE) can shed important information on understanding superconducting pairing mechanisms and superconducting electronics, reports on the GPE are few because the fabrication of the junctions with GPE is technologically difficult. Here, we report a GPE in the single-crystalline MgB_2 bilayers (*S′/S*), where the *S′* is the damaged MgB_2 layer by cobalt (Co)-ion irradiation and the *S* is the undamaged MgB_2 layer. Superconducting properties of the *S′* is remarkably degraded by the irradiation, whereas those of the *S* is uninfluenced by the irradiation. The degraded superconductivity in the *S′* is fully recovered by increasing the thickness of undamaged MgB_2 layer *S* despite almost ten times larger thickness ~ 95 nm of *S′* than the superconducting coherence length $\xi_{ab}(0)$ ~ 8.5 nm of the *S*, indicating a presence of GPE in the *S′/S* MgB_2 bilayers. A diffusion of electrons in the *S′* into the *S* can reduce a pair breaking scattering in the *S′*, and the similar electronic structures of *S′* and *S* layers and a finite attractive electron-electron interaction in the *S′* are thought to be origins of unpredicted GPE between the same superconducting materials. Both upper critical field ($\mu_0 H_{c2}$) and in-field critical current density (J_c) of *S′/S* bilayers show a significant enhancement, representing a strong correlation between *S′* and *S*. These discoveries provide the blue print to the design of the superconducting multilayers for fundamental researches on the mechanism of the GPE as well as their technological applications.

The superconducting proximity effect (PE), a leak of Cooper pairs from a superconductor (*S*) into a normal metal (*N*) when they are in contact with each other, is a fascinating phenomenon that is critical to the design of superconducting electronic devices, such as superconducting quantum interface device (SQUID) and quantum information device[1–4]. Superconducting coherence length (ξ) and electronic mean free path (l) in the normal metal are important parameters to determine the leaking distance of Cooper pairs in *S/N* junctions, which have been intensively studied and well understood based on conventional theories[2,3,5–10].

Recently, unpredicted large PE was observed when superconductor S_1 is connected with another superconductor S_2 instead of normal metal, which is known as the giant proximity effect (GPE)[11–17]. Here, superconducting transition temperature (T_c) of S_2 is lower than that of S_1. The Cooper-pair leaking distance in S_1/S_2 junctions is almost ten times larger than the coherence length ξ, and Josephson critical current could be much improved in the superconducting multilayers composed of the optimally doped and under doped high-T_c cuprates, such as LSCO ($La_{2-x}Sr_xCuO_4$)/LCO ($La_2CuO_{4+\delta}$)/LSCO trilayer[13–15]. The spatially long-ranged propagation of Cooper pairs between two different conventional superconductors, such as few-layer lead (Pb) island and Pb monolayer, was also visualized by using scanning tunnelling spectroscopy (STS) and scanning tunnelling microscopy (STM)[16,17]. The Cooper pairs' leaking distance is influenced by the T_c of S_2, which is considered due to its finite attractive interactions/phase fluctuations or an additional superconductivity between the interface of S_1 and S_2. However, the origin of GPE has yet to be clarified[12–15,18].

GPE is expected to provide a significant technological advantage for the applications of superconducting electronics because thicker barrier can make it much easier to achieve uniform Josephson junctions. GPE observed in the cuprates-based Josephson junctions, however, has shown inconsistent results partly because of the surface roughness between layers and secondary phases[13,15]. Fabrication of the uniform multilayers in such complex compounds has proven to be difficult so far.

Ion irradiations have been often used to fabricate *S/N/S* Josephson junctions because local crystal disorders or defects can easily be controlled by an irradiating ion source or its dose[19–23], and long range PE has been also

[1]Center for Quantum Materials and Superconductivity (CQMS), Sungkyunkwan University, Suwon, 16419, Republic of Korea. [2]Department of Physics, Sungkyunkwan University, Suwon, 16419, Republic of Korea. [3]Department of Materials Engineering, KU Leuven, Kasteelpark Arenberg 44-bus 2450, B-3001, Leuven, Belgium. Correspondence and requests for materials should be addressed to W.N.K. (email: wnkang@skku.edu) or T.P. (email: tp8701@skku.edu)

observed in the junctions fabricated by ion irradiations[23]. Similar electronic structures between *S* and *N* layers and a finite SC pairing interaction in the *N* layer are considered as sources for the enhanced proximity effect[13,14,16,24]. Conventional superconductor MgB_2 with relatively high T_c of 40 K is a good candidate for GPE realization via the ion irradiation technique because of its large superconducting coherence length, metallicity, and large superconducting energy gap[25,26].

Here we report the giant proximity effect in the S'/S MgB_2 bilayers. A dose of 1×10^{14} Co atoms/cm^2 with the 140 keV beam energy (mean projected range $\delta = 95$ nm), where δ is the average distance from the surface of the film at which the irradiated Co ions come to maximum concentration, is irradiated into single-crystalline MgB_2 films with various thicknesses (t) of 130, 200, 410, 850, and 1,300 nm. T_c of the MgB_2 film with $t = 130$ nm is considerably suppressed from 38.2 to 4.5 K after the Co-ion irradiation. Although, the thickness of damaged MgB_2 layer (S') by the irradiation is almost ten times longer than the coherence length, $\xi_{ab}(0) \sim 8.5$ nm, of the undamaged MgB_2 layer (S), the suppressed T_c of S' by the irradiation is rapidly restored to that of the pristine state with an increase in the thickness of S. In addition, upper critical field ($\mu_0 H_{c2}$) of the S'/S bilayers has two times larger value than that of the pristine films, and field performance of critical current density (J_c) of the bilayers is superior to that of the pristine MgB_2 films. These results demonstrate that the existence of giant proximity effect in the S'/S MgB_2 bilayers provides a blue print to fabricate superconducting MgB_2 multilayers for their fundamental researches as well as technological applications.

Results

Figure 1(a) shows the mean projected range ($\delta = 95$ nm) of the irradiated 140 keV Co ions into MgB_2 and damage events created by the irradiated energetic ions, simulated by the SRIM program[27]. If MgB_2 film is thick enough compared to the δ, it can be divided into two layers: damaged layer (S') and undamaged layer (S). Superconducting (SC) properties of the S is expected to be same with that of the pristine state, while the SC properties of the S' will be changed by the ion-irradiation conditions. In order to investigate the correlation between S' and S, we considered two types of electrode configurations, i.e., 4-point contact method A and B, as described in the insets of Fig. 1(a). In contact method A, the 4 probes are directly connected to the S, whereas they are in contact with the S' in contact method B.

The solid lines in Fig. 1(b) indicate the temperature dependences of electrical resistivity (ρ) for the pristine MB850 nm at magnetic fields of 2 and 4 T, where $\rho(T)$ is normalized by the ρ value at T_c onset, ρ_n, at each magnetic field for comparison. After irradiation with a dose of 1×10^{14} Co atoms/cm^2 in the MB850 nm, $\rho(T)$ was measured again by using the 4-point contact method A and B. For the contact method B, the resistivity drop of the irradiated film at T_c is sharper and more robust than that of the pristine: at 4 Tesla, the zero-resistance state is suppressed to 19.1 K for the irradiated film, while it is 4.8 K for the pristine. The $\rho(T)$ curves measured by the contact method A, in contrast, show two SC transitions: the first SC transition is consistent with the SC transition of the S' measured by the contact method B and the second SC transition is similar to the SC transition of the pristine sample. These results delineate that S'/S MgB_2 bilayer is fabricated via the ion irradiation method.

The $\rho(T)$ curve near T_c for pristine MgB_2 films of MB130 nm, MB200 nm, MB410 nm, MB850 nm, and MB1300 nm is shown in Fig. 2(a), where $\rho(T)$ is normalized by the ρ value at 41 K, $\rho(41\,\text{K})$. With decreasing film thickness, T_c of the pristine MgB_2 films slightly decreases and the SC transition remains sharp, except the thinnest MB130 nm (ref.[28]) (see Fig. S1 in the Supplemental Information). On the other hand, T_c of the S'/S MgB_2 bilayers is rapidly suppressed with decreasing the thickness (t') of undamaged MgB_2 layer S, as shown in Fig. 2(b), where $\rho(T)$ was measured by using the contact method A. The change in T_c of the S'/S bilayers is linked to t' because the same dose of Co ions with the same incident energy of 140 keV was irradiated. The large suppression of T_c from 38.2 to 4.5 K in MB130 nm after the irradiation indicates that a dose of 1×10^{14} Co atoms/cm^2 is enough to substantially degrade superconductivity of the MgB_2. Interestingly, however, T_c is rapidly restored back to the original value with increasing film thickness. Temperature dependences of dc magnetization (M) also showed similar results to the $\rho(T)$ curve (Fig. S2 in the Supplemental Information), indicating that the SC transition in the S'/S bilayers is not originated from filamentary nature. In addition, the fact that the thickness of damaged MgB_2 layer (S') is much larger than the coherence length (ξ) of MgB_2 (ref.[26]) indicates the emergence of giant proximity effect (GPE) in S'/S MgB_2 bilayers. We note that the GPE is often observed in S_1/S_2 junctions, where S_1 and S_2 are superconducting layers with different T_c (refs[11–17]).

Figure 2(c) displays the SC transition temperature of the irradiated MgB_2 films ($T_{c,irr.}$), normalized by that of the pristine films ($T_{c,pri.}$), as a function of the reduced film thickness t'/δ, where t' ($= t - \delta$) represents the thickness of the undamaged layer (S) and δ corresponds to the thickness of the damaged layer (S'). Here, $T_{c,pri.}$ and $T_{c,irr.}$ are determined from the criterion of 50% resistivity drop from the resistivity value at 41 K. For comparison, $T_{c,irr.}/T_{c,pri.}$ for S'/S bilayers with $\delta = 27$ (stars) and 49 nm (circles) are also plotted in Fig. 2(c), where a beam energy of 35 ($\delta \sim 27.3$ nm) and 70 keV ($\delta \sim 49.4$ nm) was used with the same dose of 1×10^{14} Co atoms/cm^2. Inset of Fig. 2(c) shows $T_{c,pri.}$ and $T_{c,irr.}$ as a function of the t'/δ for pristine and irradiated MgB_2 films, respectively. $T_{c,irr.}$ that corresponds to the T_c of S'/S bilayers is monotonically reduced with decreasing t'/δ and is completely suppressed to 0 K at the critical ratio $t'/\delta \sim 0.19$, i.e. 19% of the thickness of S to that of S'. For $\delta = 95$ nm, for instance, the critical thickness ($T_{c,irr.} = 0$ K) of the S'/S MgB_2 bilayer is 113 nm.

Discussion

The thickness ratio (t'/δ) dependence of the SC transition temperature for the S'/S bilayers is expressed by the Werthamer theory considered the spatial variation of electron-electron interaction[6], even though the thicknesses of the S and S' are much thicker than coherence length of MgB_2. In the BCS theory, T_c of a normal metal (N) and superconductor (S) bilayer can simply be expressed by the relation $T_c = 1.14\Theta_D \exp[-1/(N_0 V_0)_{eff}]$, where Θ_D is Debye temperature, N_0 is the electronic density of states at the Fermi energy, and V_0 is strength of attractive electron-electron interaction, and $(N_0 V_0)_{eff}$ is the effective BCS interaction parameter[2,6,29]. For N/S bilayer, $N_0 V_0$

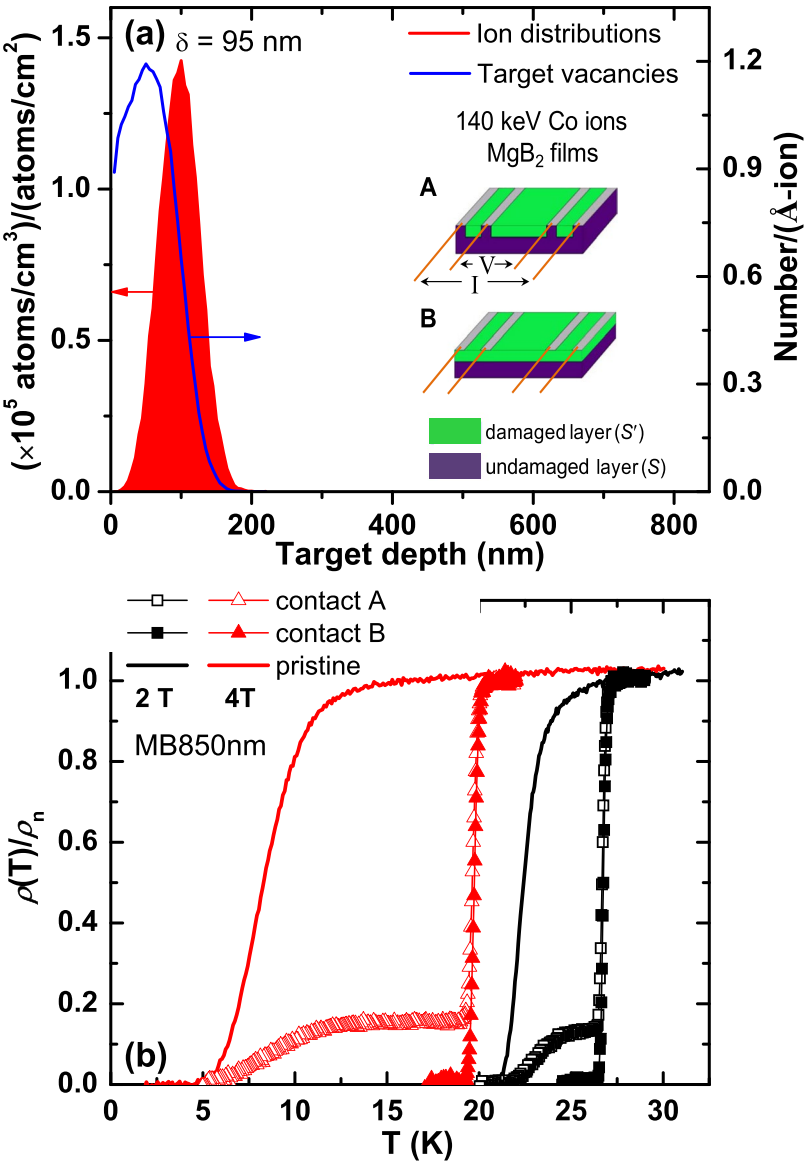

Figure 1. Schematic view of MgB_2/MgB_2 bilayers fabricated by cobalt ion irradiation. (**a**) SRIM simulation for the mean projected range (δ) and target vacancies resulted from damaged events of irradiated Co ions with an incident energy of 140 keV in MgB_2, where the estimated δ is around 95 nm. Insets show two types of configurations for the four-probe point contacts: contact method A and B. Electrical resistivity (ρ) measured by the contact method A is influenced by both damaged layer (S') and undamaged layer (S). On the other hand, the SC transition measured by the contact method B is determined by the S'. (**b**) Temperature dependences of the normalized resistivity, $\rho(T)/\rho_n$, for the pristine and irradiated MB850 nm at magnetic fields of 2 and 4 T, where ρ_n is the resistivity at T_c onset at each magnetic field. The kinks and the second SC transitions observed from the contact method A are due to the undamaged layer S, indicating the formation of the S'/S MgB_2 bilayer via the Co-ion irradiation.

in the S layer is an important parameter to determine T_c of the bilayer, because $V_0 = 0$ in the N layer. On the other hand, a finite V_0 in the N layer could induce the long range of the PE due to the slow decay of SC pair amplitude in the N layer[16,18,24], which is probably one of the primary reasons for GPE in the S'/S MgB_2 bilayer.

The electronic density of states at the Fermi energy (N_0) is also important to determine T_c, and the large reduction of T_c in MgB_2 by the irradiation is believed to be due to the decreased N_0 and enhanced interband scattering[30–34]. Considering a significant decrease of T_c of MB130 nm from 38.2 to 4.5 K by Co-ion irradiation, the T_c variation in the S'/S MgB_2 bilayers is expressed by the decrease in the N_0 (refs[29,35,36]). Figure 2(d) shows that the inverse of T_c difference between the pristine and irradiated films, $1/\Delta T_c$ ($=T_{c,pri.} - T_{c,irr.}$), is linearly proportional to the thickness ratio between the undamaged (t') and damaged MgB_2 layers (δ), t'/δ, indicating that the T_c suppression by the Co-ion irradiation is closely related with the decrease in the electronic density of states N_0 of the damaged layer S' (refs[29,35,36]). The initial slope of T_c ($\propto |dT_c(d_n = 0)/dd_n|$) in S/N bilayer is proportional to the ratio of density of states between the two layers (N_n/N_s) because $T_c = 1.14\,\Theta_D \exp[-1/(N_0 V_0)]$, where N_n and N_s are the

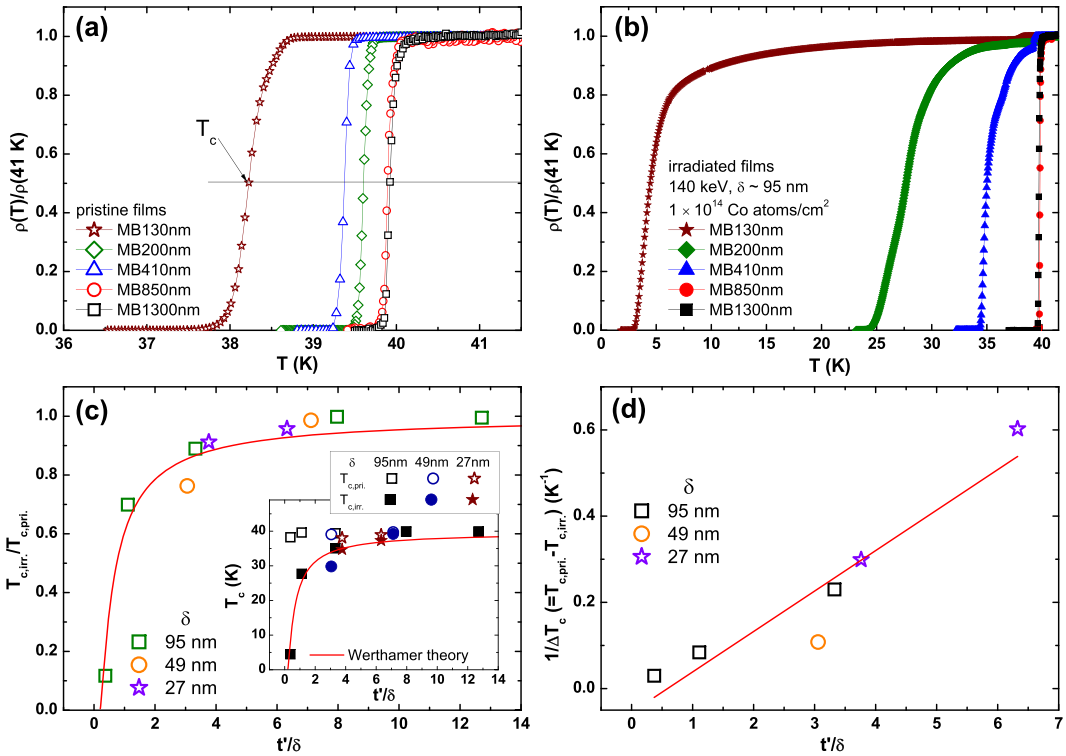

Figure 2. Thickness dependence of superconducting transition temperature for irradiated MgB_2 films. $\rho(T)$ curves near the SC transitions for (**a**) pristine and (**b**) Co-ion irradiated MB130 nm, MB200 nm, MB410 nm, MB850 nm, and MB1300 nm, where $\rho(T)$ was normalized by the ρ at 41 K, $\rho(41\,K)$, for comparison. (**c**) The SC transition temperature of the irradiated films ($T_{c,irr.}$) as a function of t'/δ, where the $T_{c,irr.}$ is normalized by T_c of the pristine films ($T_{c,pri.}$) and t' ($=t-\delta$) is the thickness of the *S*. Star, circle, and square symbols represent T_cs for different incident energies of 35 ($\delta \sim 27$ nm), 70 ($\delta \sim 49$ nm), and 140 keV ($\delta \sim 95$ nm), respectively. Both $T_{c,pri.}$ and $T_{c,irr.}$ are determined from the midpoint of SC transition, $\rho_{50\%}$, 50% resistivity drop from the ρ_n. The red solid line is a fitting curve by using the Werthamer theory. Inset shows the $T_{c,pri.}$ and $T_{c,irr.}$ as a function of t'/δ. (**d**) The inverse of the T_c reduction, $1/\Delta T_c$ ($=T_{c,pri.} - T_{c,irr.}$), is plotted as a function of t'/δ.

density of states at the Fermi energy for the normal and superconducting layer, respectively, and d_n is a thickness of the normal layer[29,35,36]. Our results on the T_c reduction with respect to the thickness ratio t'/δ is consistent with the decrease in the density of states of the S' caused by the irradiation-induced disorder[30–34].

We consider the diffusion of electrons inside the damaged S' into the undamaged *S* as well as the diffusion of Cooper pairs from the *S* to S'. Those diffusion processes by the electrons and the Cooper pairs can lead the extension of the proximity region in terms of the strong correlation between *S* and S'. In particular, when the thickness of *S* is large, there can be enough space for the diffusion of electrons from the S' into *S*. This interpretation is supported by the study on the lower and upper critical fields and critical current density for S'/S MgB_2 bilayers, which will be discussed below.

Figure 3(a,b) show the $\rho(T)$ curves in magnetic fields for the pristine and Co-ion irradiated MB410 nm, respectively, where the $\rho(T)$ is normalized by the resistivity value in the normal state (ρ_n) for each magnetic field. In stark contrast to the pristine film, two-step SC transitions appear in the $\rho(T,H)$ measured by the 4-probe contact method A for the Co-ion irradiated MB410 nm. The second SC transition temperature (T_{c2}) is consistent with the SC transition temperature of pristine films ($T_{c,pri.}$), indicating that T_{c2} emerged at high magnetic fields is originated from superconductivity in the *S*. When the contact method B was used, on the other hand, there is no trace of T_{c2} in $\rho(T,H)$ curves because the 4 probes of the contact method B are not directly in contact with the undamaged layer and the supercurrent flows mainly through the damaged layer S'.

Temperature dependences of the upper critical field ($\mu_0 H_{c2}$) for the pristine and irradiated MB410 nm and MB850 nm are presented in Fig. 3(c,d), respectively, where the magnetic field is applied perpendicular to the film's *ab* plane ($H \perp ab$). The criteria for $T_{c,pri.}$ and $T_{c,irr.}$ are 50% resistivity drop for the pristine and irradiated films, respectively, while T_{c2}, and T_k are assigned as the 50% resistivity drop of the second SC transition and a kink temperature of the first SC transition, respectively (see the arrows in Fig. 3(a,b)). The magnetic field dependence of the kink temperature (T_k) for the MB410 nm suggests that T_k is associated with T_c of the undamaged layer *S*. One the other hand, there is no kink (T_k) in the irradiated MB850 nm because superconductivity of the damaged layer S' is completely restored to that of the pristine state, i.e., $T_{c,pri.} \approx T_{c,irr.}$. The fact that $\mu_0 H_{c2}(T)$s determined by T_{c2} are consistent with those estimated from the $T_{c,pri.}$ underscores that the MgB_2/MgB_2 bilayer is formed by the Co-ion irradiation. Upper critical field of the bilayers is enhanced by two times to the pristine films: $\mu_0 H_{c2}(0) = 5.29 \rightarrow 9.75$ T for MB410 nm and $\mu_0 H_{c2}(0) = 4.52 \rightarrow 9.50$ T for MB850 nm, which can be accounted for by additional

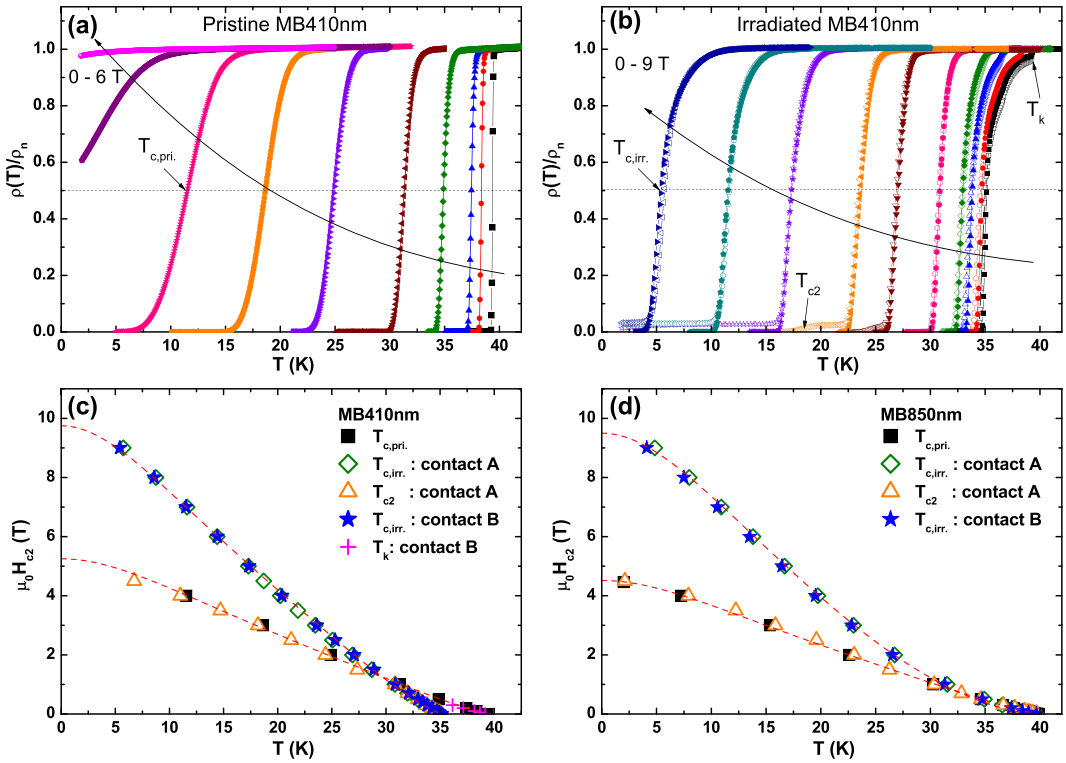

Figure 3. Upper critical fields of MgB_2/MgB_2 bilayers. $\rho(T)$ curves for (**a**) pristine and (**b**) Co-ion irradiated MB410 nm in magnetic fields, where $\rho(T)$ was normalized by the ρ_n at each magnetic field. In (**b**), the open and solid symbols are obtained from the contact method A and B, respectively. Temperature dependence of upper critical field, $\mu_0 H_{c2}(T)$, for (**c**) MB410 nm and (**d**) MB850 nm. Criteria for $T_{c,pri.}$, $T_{c,irr.}$, T_{c2}, and T_k are indicated by arrows in (**a**,**b**). The red dashed lines are obtained from the two-band Ginzburg-Landau theory. The T_{c2}'s obtained from the second SC transition are consistent with $T_{c,pri.}$, demonstrating that the irradiated films are composed of the S'/S bilayer: damaged MgB_2 layer (S') and undamaged MgB_2 layer (S).

defects introduced via the Co-ion irradiation[37]. The SC coherence length, $\xi_{ab}(0)$, obtained from the $\mu_0 H_{c2}(0)$ $[=\phi_0/2\pi\xi^2_{ab}(0)]$ is reduced from 7.89 to 5.81 nm and from 8.54 to 5.89 nm for MB410 nm and MB850 nm after the irradiation, respectively.

Temperature dependence of $\mu_0 H_{c2}$ is reasonably explained by the two-band Ginzburg-Landau theory, indicated by the red dashed lines in Fig. 3(c,d). According to Takahashi-Tachiki model in S_1/S_2 superlattices, an upturn behavior in $H_{c2}(T)$ can be observed near T_c due to different spatial variations in the density of states, the diffusion constant, and the electron-electron attractive interaction potential between S_1 and S_2 (refs[38,39]). The enhanced upturn feature of $\mu_0 H_{c2}(T)$ in the MgB_2 bilayer (MB850 nm) compared to that in the pristine film may be closely associated with the different diffusion constant between S and S' layers because $T_{c,pri.} \approx T_{c,irr.}$ in the MB850 nm. The Cooper pairs in the damaged layer may be more effective in penetrating into the undamaged layer, inverse proximity effect[16,23], than the reversal process because of a larger diffusion constant in the S than S' layer, leading to the large upturn feature in $\mu_0 H_{c2}(T)$ near T_c. On the other hand, Ferrando *et al.* suggested that a large upward behavior of $H_{c2}(T)$ near T_c in MgB_2 thin films is associated with a large resistive surface layer of MgB_2 due to the contamination in air rather than the multiband effect of MgB_2 (refs[40,41]). In order to confirm this mechanism, however, further measurements for $\mu_0 H_{c2}(T)$ in high magnetic field parallel to the *ab* plane ($H//ab$) will be needed because this upturn behavior or sudden change of $\mu_0 H_{c2}(T)$ in S'/S is more prominent for $H//ab$ (refs[38,39]).

Magnetic field dependences of critical current density (J_c) for the pristine and irradiated MgB_2 films at 5 and 20 K are shown in Fig. 4(a,b), respectively, where the magnetic field is applied perpendicular to the film's *ab* plane. The large J_c at zero field and its rapid suppression in magnetic fields indicate that the pristine MgB_2 films used in this study is clean[42,43]. After Co-ion irradiation, in-field J_c is significantly improved except for the thinnest MB130 nm film because of the large suppression of T_c. The suppression of zero-field J_c for the irradiated MB410 nm is also related with the suppressed T_c by the irradiation. On the other hand, in-field J_c for both MB850 nm and MB1300 nm is remarkably enhanced without the suppression of the zero-filed J_c after Co-ion irradiation, suggesting that the proximity effect (PE) in the S'/S bilayers is not confined near the interface[11–13], but is long ranged over the whole thickness of the irradiated layer S' when the thickness of the S is sufficiently larger than that of the S'. In addition, the large in-field J_c in S'/S MgB_2 bilayers manifests the strong correlation between S' and S layers.

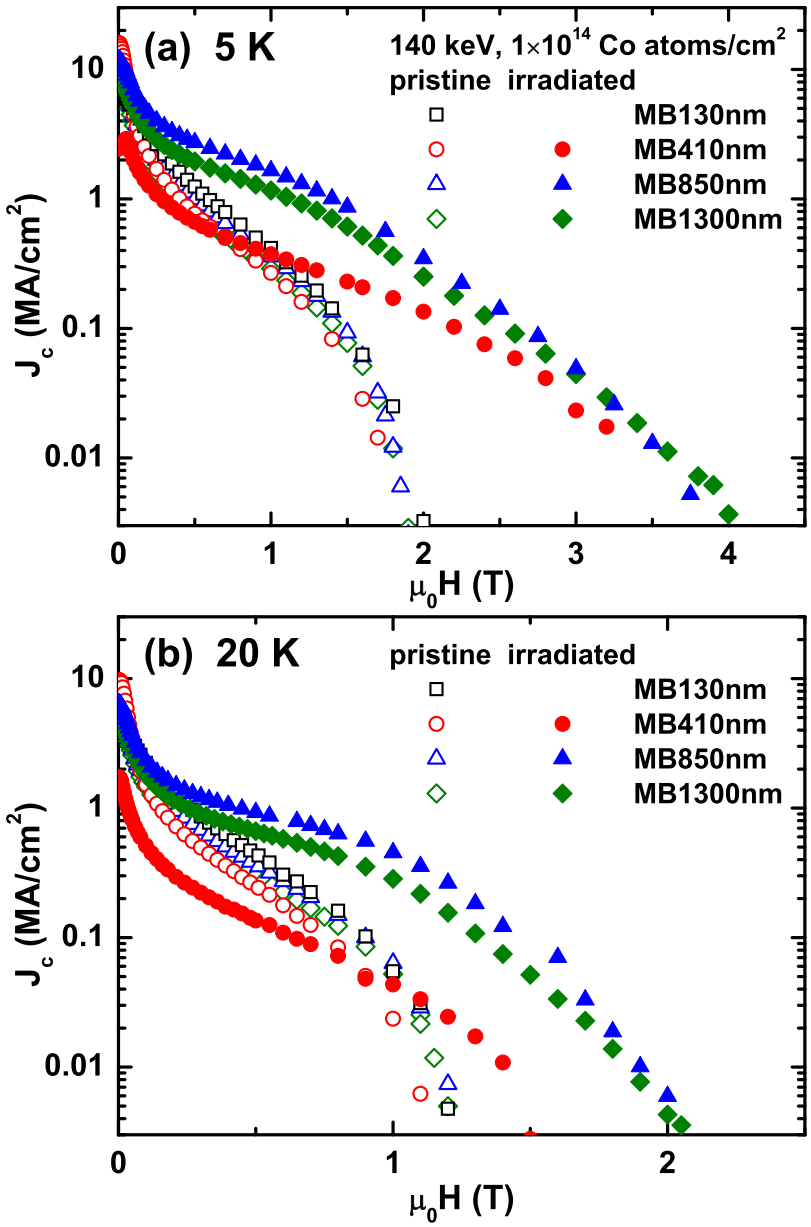

Figure 4. Critical current density, J_c, of MgB_2/MgB_2 bilayer. Magnetic field dependences of the critical current density (J_c) at (**a**) 5 and (**b**) 20 K for the pristine and Co-ion irradiated MB130 nm, MB410 nm, MB850 nm, and MB1300 nm. J_c for all pristine films shows a similar field performance, and a rapid decrease of J_c in magnetic fields indicates that the MgB_2 films used in this study is of high quality. A significant enhancement of in-field J_c after irradiation is observed except for the MB130 nm. There is no data for the J_c of the irradiated MB130 nm due to a substantially suppressed T_c and SC volume fraction.

Conclusion

In conclusion, we reported fabrication of MgB_2/MgB_2 bilayers, where a dose of 1×10^{14} Co atoms/cm^2 with a beam energy of 140 keV is irradiated into single-crystalline MgB_2 films and created the damaged layer (S') interfaced with the undamaged layer (S). Superconductivity of MgB_2 in the damaged layer is significantly weakened: T_c is suppressed from 38.2 to 4.5 K for the irradiated MB130 nm film. The suppressed superconductivity, however, was restored to the original SC state when the thickness of the undamaged MgB_2 layer (S) is sufficiently larger than that of the damaged MgB_2 layer (S'). Although the coherence length of the undamaged layer S (~8.5 nm) is more than ten times shorter than the damaged layer S' (~95 nm), the proximity effect occurs over the whole thickness of the S'. This anomalously long-ranged proximity effect in S'/S MgB_2 bilayers is thought to be originated from the similar electronic structures of S' and S layers and a finite SC pairing interaction in the S' layer. The discovery of giant proximity effect (GPE) in the MgB_2/MgB_2 bilayers is expected to provide a blue print to the design of superconducting MgB_2 multilayers for their fundamental researches as well as technological applications.

Methods

Hybrid physical-chemical vapour deposition (HPCVD) method was used for the growth of single-crystalline MgB_2 films on the *c*-cut Al_2O_3 substrates, and the details of the growth technique and the film's single-crystal quality are described elsewhere[43,44]. The MgB_2 films with various thicknesses (t) of 130 (MB130 nm), 200 (MB200 nm), 410 (MB410 nm), 850 (MB850 nm), and 1,300 nm (MB1300 nm) were fabricated for ion irradiations, and the same amount of dose of 1×10^{14} Co atoms/cm^2 with 140 keV beam energy at room temperature was irradiated into the prepared MgB_2 films in Korea Multi-purpose Accelerator Complex (KOMAC). The mean projected range (δ) of irradiated Co ions is around 95 nm, which is simulated by the Monte Carlo simulation program SRIM (The Stopping and Range of Ions in Matter)[27].

The formation of S'/S MgB_2 bilayers by the Co-ion irradiation was confirmed by simultaneously measuring electrical resistivity (ρ) of the damaged and undamaged MgB_2 layers in Physical Property Measurement System (PPMS 9 T, Quantum Design). The standard 4-probe method was used for electrical resistivity measurements, and the 4-point contact regions were protected from the irradiation by using gold (Au) coating and silver (Ag) epoxy in order to measure the resistivity of the undamaged layer after the irradiation. In order to estimate the critical current density (J_c), magnetization hysteresis ($M - H$) loops were measured by using a Magnetic Property Measurement System (MPMS 5 T, Quantum Design) before and after the Co-ion irradiations (see Fig. S3 in the Supplemental Information).

References

1. Meissner, H. Superconductivity of contacts with interposed barriers. *Phys. Rev.* **117**, 672 (1960).
2. de Gennes, P. G. Boundary effects in superconductors. *Rev. Mod. Phys.* **36**, 225 (1964).
3. Likharev, K. K. Superconducting weak links. *Rev. Mod. Phys.* **51**, 101 (1979).
4. Makhlin, Y., Schön, G. & Shnirman, A. Quantum-state engineering with Josephson-junction devices. *Rev. Mod. Phys.* **73**, 357 (2001).
5. Hilsch, P. & Hilsch, R. Zur Supraleitung von Schichtpaketen aus Normal- und Supraleitern. *Z. Phys.* **180**, 10 (1964).
6. Werthamer, N. R. Theory of the superconducting transition temperature and energy gap function of superposed metal films. *Phys. Rev.* **132**, 2440 (1963).
7. Kircher, C. J. Superconducting proximity effect of Nb. *Phys. Rev.* **168**, 437 (1968).
8. Hauser, J. J., Theuerer, H. C. & Werthamer, N. R. Superconductivity in Cu and Pt by means of superimposed films with lead. *Phys. Rev.* **136**, A637 (1964).
9. de Gennes, P. G. & Guyon, E. Superconductivity in "normal" metals. *Phys. Lett.* **3**, 168 (1963).
10. Kim, J., Doh, Y.-J., Char, K., Doh, H. & Choi, H.-Y. Proximity effect in Nb/Au/CoFe trilayers. *Phys. Rev. B* **71**, 214519 (2005).
11. Decca, R. S., Drew, H. D., Osquiguil, E., Maiorov, B. & Guimpel, J. Anomalous proximity effect in underdoped $YBa_2Cu_3O_{6+x}$ Josephson junctions. *Phys. Rev. Lett.* **85**, 3708 (2000).
12. Marchand, D., Covaci, L., Berciu, M. & Franz, M. Giant proximity effect in a phase-fluctuating superconductor. *Phys. Rev. Lett.* **101**, 097004 (2008).
13. Bozovic, I. *et al*. Giant proximity effect in cuprate superconductors. *Phys. Rev. Lett.* **93**, 157002 (2004).
14. Covaci, L. & Marsiglio, F. Proximity effect and Josephson current in clean strong/weak/strong superconducting trilayers. *Phys. Rev. B* **73**, 014503 (2006).
15. Rout, P. K. & Budhani, R. C. Interface superconductivity in $La_{1.48}Nd_{0.4}Sr_{0.12}CuO_4/La_{1.84}Sr_{0.16}CuO_4$ bilayers. *Phys. Rev. B* **82**, 024518 (2010).
16. Cherkez, V. *et al*. Proximity effect between two superconductors spatially resolved by scanning tunneling spectroscopy. *Phys. Rev. X* **4**, 011033 (2014).
17. Kim, J. *et al*. Visualization of geometric influences on proximity effects in heterogeneous superconductor thin films. *Nat. Phys.* **8**, 464 (2012).
18. Quintanilla, J., Capelle, K. & Oliveira, L. N. Comment on "Anomalous proximity effect in underdoped $YBa_2Cu_3O_{6+x}$ Josephson junctions". *Phys. Rev. Lett.* **90**, 089703 (2003).
19. Kahlmann, F. *et al*. Superconductor–normal–superconductor Josephson junctions fabricated by oxygen implantation into $YBa_2Cu_3O_{7-\delta}$. *J. Appl. Phys. Lett.* **73**, 2354 (1998).
20. Cybart, S. A. *et al*. Planar MgB_2 Josephson junctions and series arrays via nanolithography and ion damage. *Appl. Phys. Lett.* **88**, 012509 (2006).
21. Kang, D.-J. *et al*. Realization and properties of $YBa_2Cu_3O_{7-\delta}$ Josephson junctions by metal masked ion damage technique. *Appl. Phys. Lett.* **80**, 814 (2002).
22. Sirena, M. *et al*. Annealing of ion irradiated high T_c Josephson junctions studied by numerical simulations. *J. Appl. Phys.* **105**, 023910 (2009).
23. Sharafiev, A. *et al*. HTS Josephson junctions arrays for high-frequency mixing. *Supercond. Sci. Technol.* **31**, 035003 (2018).
24. Tachiki, M. & Takahashi, S. Proximity effect in high-T_c oxide superconductors. *Physics C* **191**, 363 (1992).
25. Cybart, S. A. *et al*. Large scale two-dimensional arrays of magnesium diboride superconducting quantum interference devices. *Appl. Phys. Lett.* **104**, 182604 (2014).
26. Galan, E., Cunnane, D., Xi, X. X. & Chen, K. Sandwich-type $MgB_2/TiB_2/MgB_2$ Josephson junctions. *Supercond. Sci. Technol.* **27**, 065015 (2014).
27. *The projected range of Co ions in the MgB_2 film was calculated using the SRIM software*. (www.srim.org/).
28. Pogrebnyakov, A. V. *et al*. Thickness dependence of the properties of epitaxial thin films grown by hybrid physical-chemical vapor deposition. *Appl. Phys. Lett.* **82**, 4319 (2003).
29. Zhang, M., Tateishi, G. & Bergmann, G. Discrepancies between experiment and theory in the superconducting proximity effect. *Phys. Rev. B* **74**, 014506 (2006).
30. Ferrando, V. *et al*. Neutron irradiation effects on two gaps in MgB_2. *Physica C* **456**, 144 (2007).
31. Gerashenko, A. P., Mikhalev, K. N., Verkhovskii, S. V., Karkin, A. E. & Goshchitskii, B. N. Reduction in the electron density of states in superconducting MgB_2 disordered by neutron irradiation: ^{11}B and ^{25}Mg NMR estimates. *Phys. Rev. B* **65**, 132506 (2002).
32. Vinod, K., Varghese, N. & Syamaprasad, U. Superconductivity of MgB_2 in the BCS framework with emphasis on extrinsic effects on critical temperature. *Supercond. Sci. Technol.* **20**, R31 (2007).
33. Putti, M., Vaglio, R. & Rowell, J. M. Radiation effects on MgB_2: a review and a comparison with A15 superconductors. *Supercond. Sci. Technol.* **21**, 043001 (2008).
34. Putti, M. *et al*. Intraband vs. interband scattering rate effects in neutron irradiated MgB_2. *EPL* **77**, 57005 (2007).
35. Bergmann, G. Quantitative simulation of the superconducting proximity effect. *Phys. Rev. B* **72**, 134505 (2005).
36. Garrett, D., Zhang, M. & Bergmann, G. The superconducting proximity effect as a tool to investigate metal films and interfaces. *Eur. Phys. J. B* **39**, 199 (2004).
37. Tinkham, M. *Introduction to Superconductivity*, 2nd ed (McGraw- Hill, New York, 1996).
38. Takahashi, S. & Tachiki, M. Theory of the upper critical field of superconducting superlattices. *Phys. Rev. B* **33**, 4620 (1986).

39. Takahashi, S. & Tachiki, M. New phase diagram in superconducting superlattices. *Phys. Rev. B* **34**, 3162 (1986).
40. Ferrando, V. *et al*. Systematic study of disorder induced by neutron irradiation in MgB_2 thin films. *J. Appl. Phys.* **101**, 043903 (2007).
41. Gurevich, A. Enhancement of the upper critical field by nonmagnetic impurities in dirty two-gap superconductors. *Phys. Rev. B* **67**, 184515 (2003).
42. Hanna, M. *et al*. Clean epitaxial MgB2 films fabricated by the *ex situ* annealing of chemical vapour deposition-grown B films in Mg vapour. *Supercond. Sci. Technol.* **21**, 045005 (2008).
43. Jung, S.-G., Seong, W. K. & Kang, W. N. Flux pinning mechanism in single-crystalline MgB_2 thin films. *J. Phys. Soc. Jpn.* **82**, 114712 (2013).
44. Seong, W. K., Oh, S. & Kang, W. N. Perfect domain-lattice matching between MgB_2 and Al2O3: Single-crystal MgB_2 thin films grown on sapphire. *Jpn. J. Appl. Phys.* **51**, 083101 (2012).

Acknowledgements

We wish to acknowledge the outstanding support of the accelerator group and operators of KOMAC (Korea Multi-purpose Accelerator Complex), KAERI. This work was supported by the National Research Foundation (NRF) of Korea by a grant funded by the Korean Ministry of Science, ICT and Planning (No. 2012R1A3A2048816) and the Basic Science Research Program through the National Research Foundation of Korea (NRF) funded by the Ministry of Education (NRF-2016R1D1A1B03934513, NRF-2015R1D1A1A01060382, and 2018R1D1A1B07048987).

Author Contributions

S.-G.J. conceived the work and performed the transport and magnetization measurements. D.P. and W.N.K. fabricated single-crystalline MgB_2 thin films. S.-G.J., T.-H.P., H.-Y.C. and J.W.S. analysed the data and discussed the results with all authors. The manuscript was written by S.-G.J., W.N.K. and T.P. with inputs from all authors.

Additional Information

Supplementary information accompanies this paper at https://doi.org/10.1038/s41598-019-40263-9.

Competing Interests: The authors declare no competing interests.

Publisher's note: Springer Nature remains neutral with regard to jurisdictional claims in published maps and institutional affiliations.